22% efficient dopant-free interdigitated back contact silicon solar cells

Weiliang Wu[1,2], Wenjie Lin[1], Sihua Zhong[2], Bertrand Paviet-Salomon[3], Zongcun Liang*[1,4,a)], Mathieu Boccard[2], Hui Shen*[1,4,b)] and Christophe Ballif[2,3]

[1] *Institute for Solar Energy Systems, School of Physics and State Key Laboratory of Optoelectronic Materials and Technologies, Sun Yat-Sen University (SYSU), Guangzhou, China.*
[2] *Photovoltaics and Thin Film Electronics Laboratory, Institute of Microengineering, École Polytechnique Fédérale de Lausanne (EPFL), Rue de la Maladière 71b, CH-2000 Neuchâtel, Switzerland.*
[3] *Centre Suisse d'Électronique et de Microtechnique (CSEM), PV-Center, Rue Jaquet-Droz 1, CH-2002 Neuchâtel, Switzerland.*
[4] *Shunde-SYSU Institute for Solar Energy, Shunde, China .*

Corresponding author:[(a)] liangzc@mail.sysu.edu.cn
[(b)] shenhui1956@163.com

Abstract. In this study, we present dopant-free back contact heterojunction silicon solar cells employing MoO_x and MgF_x based stacks as hole- and electron-selective contacts deposited using a thermal evaporation process at low temperature. Only two masking steps and one alignment are required in this simple process flow. We investigate the effect of varying the MgF_x film thickness as the electron contact layer on the rear side on IBC Si solar cells and define an optimal thickness of 1.5 nm of MgF_x for high V_{OC} and *FF*. We compare different electron-selective contact materials including Mg-based and fluoride materials and discuss the suitable combinations. We fabricate dopant-free back contact solar cells by applying a stack of 1.5 nm MgF_2/70 nm Al/800 nm Ag films on intrinsic a-Si:H, maintaining excellent passivation and show efficient carrier extraction. A 4.5-cm^2 dopant-free back contact solar cells fabricated with these layers enables high V_{OC} up to 709 mV and *FF* up to 75.6% still limited by series resistance due to too thin metal layers, a pseudo *FF* of 84.2% is yet measured. The cell exhibits very low front reflection and has outstanding collection efficiency, the *IQE* reach 98.2% - 99% ranging from 600 to 900-nm due to low recombination of MoO_x and MgF_x contacts results in a high J_{SC} of 41.5 mA/cm^2.

INTRODUCTION

The interdigitated back-contact (IBC) solar cells architecture was proposed in 1970s [1]. Upon successive improvements of this technology, an efficiency over 25% and an open-circuit voltage (V_{OC}) of 737 mV under standard test condition (STC) operation have been demonstrated [2]. One major advantage of IBC solar cells is that a high short-circuit current density (J_{SC}) can be achieved by eliminating front-side metal grid shading and using a broadband antireflection stacked films [3]. IBC solar cells thus have a strong potential to reach ultra-high efficiencies. For standard IBC fabrication process, high-temperature boron and phosphorus diffusion are applied to the back surface to selectively transport holes and electrons. The electron- and hole- contacts are both localized to reduce the surface recombination rate of dopant surface [4,5], and an IBC solar cell consists of interdigitated stripes of selective n-type and p-type regions formed by the laser-doped [6], screen-printed etch mask [7] or photolithography process [4]. One possible limitation to the efficiency for IBC solar cells is the passivated contacts, notably highly-doped homo-junctions leading to potential sources of loss such as free carrier absorption (FCA), Auger recombination, Shockley–Read–Hall (SRH) recombination.

The present development of HBC solar cells still relies on the heavily doped amorphous Si (a-Si) layers, which are fabricated using inflammable and explosive precursor gases such as semiconductor-grade silane (SiH_4), phosphine (PH_3), and diborane (B_2H_6) diluted in H_2. Dopant-free, back-contacted c-Si solar cell have been developed employing

dopant-free asymmetric hetero-contacts fabricated using relatively simple technique by evaporation, potentially reducing the cost and complexity of fabrication. The high defect density at the silicon surfaces is so far limiting the open-circuit voltage (V_{OC}) to 561 mV [8,9,13]. On the other hand, fully dopant-free passivated two-side contacted silicon solar cells with efficiency up to 20.7% have been achieved with a V_{OC} of 716 mV. Inspired by these, we developed a simple approach to fabricate dopant-free, passivated interdigitated back contact (IBC) solar cells using intrinsic a-Si:H as back surface interfacial passivation layer, MoO_x as hole-selective contact and MgF_x/Al stacks as electron-selective contacts. Both polarities are fabricated by thermal evaporation, requiring only two masking steps and a single alignment procedure.

METHODOLOGY

Figure 1 shows dopant-free IBC solar cells on n-type (100) oriented float-zone silicon wafers (2.5 Ω cm, 240 µm). A 5-nm-thick a-Si:H-(i) layer was deposited by plasma enhanced chemical vapor deposition (PECVD) on both sides of the wafer, and a DARC (double antireflection coating) films consisting of 50 nm SiN_x followed by 90 nm thick MgF_x was deposited by PECVD at a substrate temperature of 200 °C and room-temperature. A metal mask patterning process was employed in the present study to fabricate IBC solar cells featuring hole- and electron-selective contacts in lieu of the usual photolithography. As shown in Fig. 1 (c), for the rear-side contacts, an 8-nm-thick MoO_x and 800-nm-thick Ag layers were applied by thermal evaporation conducted at a room temperature with a deposition rate of about 0.2–0.5 Å/s at a base pressure of 1.0×10^{-5} Torr with in-situ metal mask 1. The 1.5 nm MgF_x/ 35 nm Al / 800 nm Ag films were thermally evaporated onto the wafer substrate with the in-situ metal shadow mask 2 as shown in Fig 1 (d). A precise alignment was obtained by this simple process, forming a uniform 200 µm gap between the MoO_x/Ag and MgF_x/Al/Ag contacts. The contact area were 240 µm in half-width and 750 µm in half-width for the electron- and hole-contact, respsectively.

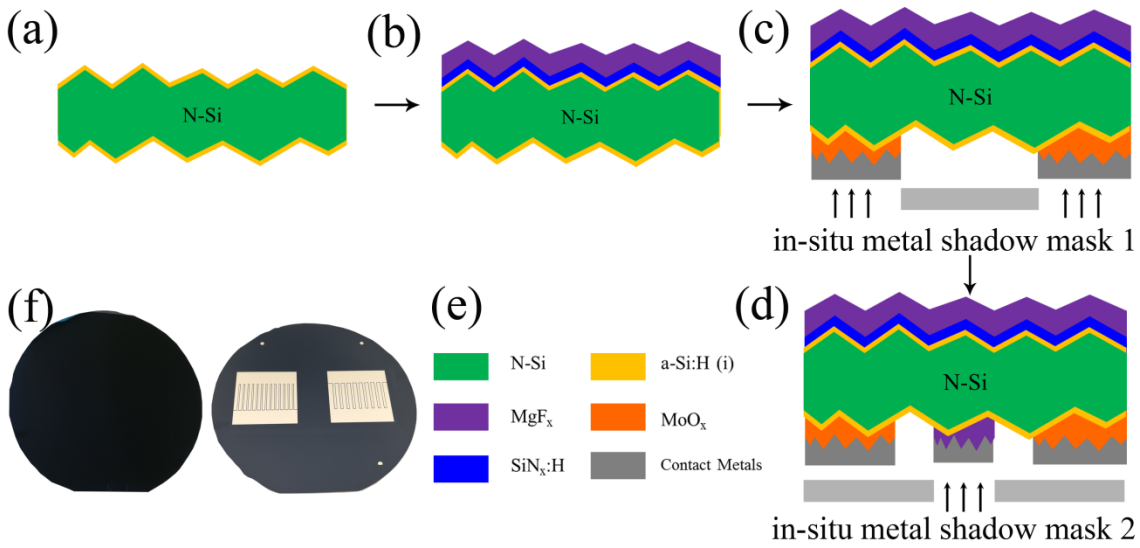

FIGURE 1. (a) - (e) Schematic diagram of the dopant free IBC solar cell process flow. (f) Optical image of IBC solar cell front- and rear-side with interdigitated MoO_x/Ag and MgF_x/Al/Ag contacts.

Fig. 1(f) shows the MLBC solar cell with the hole selective contact fraction of 55% and 60% in order to balance the influence of back contact cell geometry on contact resistivity and contact recombination. The rear-side interdigitated contacted fraction area (fHTL) of 60% has the pitch of 1500 µm corresponds to a hole contacted half-width of 800 µm and a electron contacted half-width of 500 µm,the fHTL of 55% has the reduced pitch of 1100 µm corresponds to a hole contacted half-width of 750 µm and a reduced electron contacted half-width of 250 µm. The 1.5 nm MgFx/ 35 nm Al / 800 nm Ag films were thermally evaporated onto the wafer substrate with the in-situ metal

shadow mask 2 as shown in Fig 1 (d). The Fig. 1 (f) shows the optical image of IBC solar cell front- and rear-side with interdigitated MoO_x/Ag and MgF_x/Al/Ag contacts.

The light J-V behavior was employed on a Wacom solar simulator sourcemeter under standard one sun conditions (100 mW/cm^2, AM1.5 spectrum, 25 °C) and *J-V* curves were recorded by Keithley 2601A with a 1.5 × 3 cm^2 aperture mask. The External Quantum Efficiency (*EQE*) was conducted using an in-house built setup system. The J_{SC} of the cell was integrated from *EQE* measurement. The injection level dependent open-circuit voltage was measured by transient photo-conductance measurement (WCT-120, Sinton).

RESULTS AND DISCUSSION

Due to the long path towards the contacts, the passivation plays a critical role in the carrier collection efficiency. Also, primary reflection has to be optimized to reduce at maximum optical losses. Figure 2 shows the reflectance of front surface with different anti-reflection films and calculated for random pyramids with a base angle of 45° prepared by the HNO_3/HF smooth. A lower reflectance can be achieved by utilising a double antireflection coating (ARC) consisting of a 100 nm MgF_2/45 nm ZnS or 90 nm MgF_2 /50 nm SiN_x (n = 1.96), as compared with a single-layer 80 nm SiN_x or 110 nm MgF_x. In Fig. 2 (b), the *i*-V_{oc} values are as a function of the front-side different anti-reflection film. It can be seen that in this experiment a maximum *i*-V_{oc} of 735 mV is obtained for the 80 nm SiN_x and 90 nm MgF_2 /50 nm SiN_x (n = 1.96) films. The a-Si:H (i) layer capped with SiN_x and MgF_2 is thus an excellent stack to passivate the front interface defects and provide low primary reflectance.

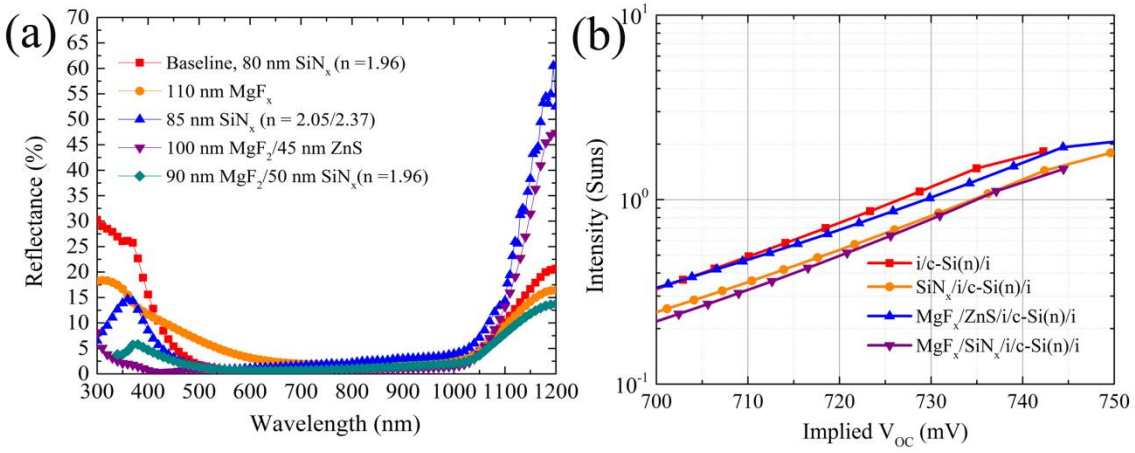

FIGURE 2. (a) The reflectance of IBC solar cells with different antireflection films; (b) The implied-V_{oc} (*i*-V_{oc}) values are as a function of the front-side different anti-reflection films.

Figure 3 shows the dependence of the characterized performance for the dopant-free IBC solar cells with 7.5 nm a-Si:H (i)/MgF_x/Al as electron contact. A strong dependence on the MgF_x thickness in the 0.6 - 2 nm range can be observed. The best efficiency in the vicinity of 20.5% have also been achieved on the small size cell (A = 0.84 cm^2). As shown in Fig. 3 (a) (c), the V_{OC} and *FF* increases with increasing thickness of MgF_x until 1.5 nm, and a high value of 725 mV can be achieved, which can be attributed to the lowest contact resistivity of 80 mΩ cm^2 [14]. As shown in Fig. 3 (b), the J_{SC} losses follow the same trend as V_{OC}, indicating that for these devices *Jsc* is mainly driven by the electrical shading effect due to low charge carrier collection probability. The high J_{SC} of 40.8 mA/cm^2 is within expectations since this cell features an MgF_x/SiN_x stacked films as antireflection and passivation coatings.

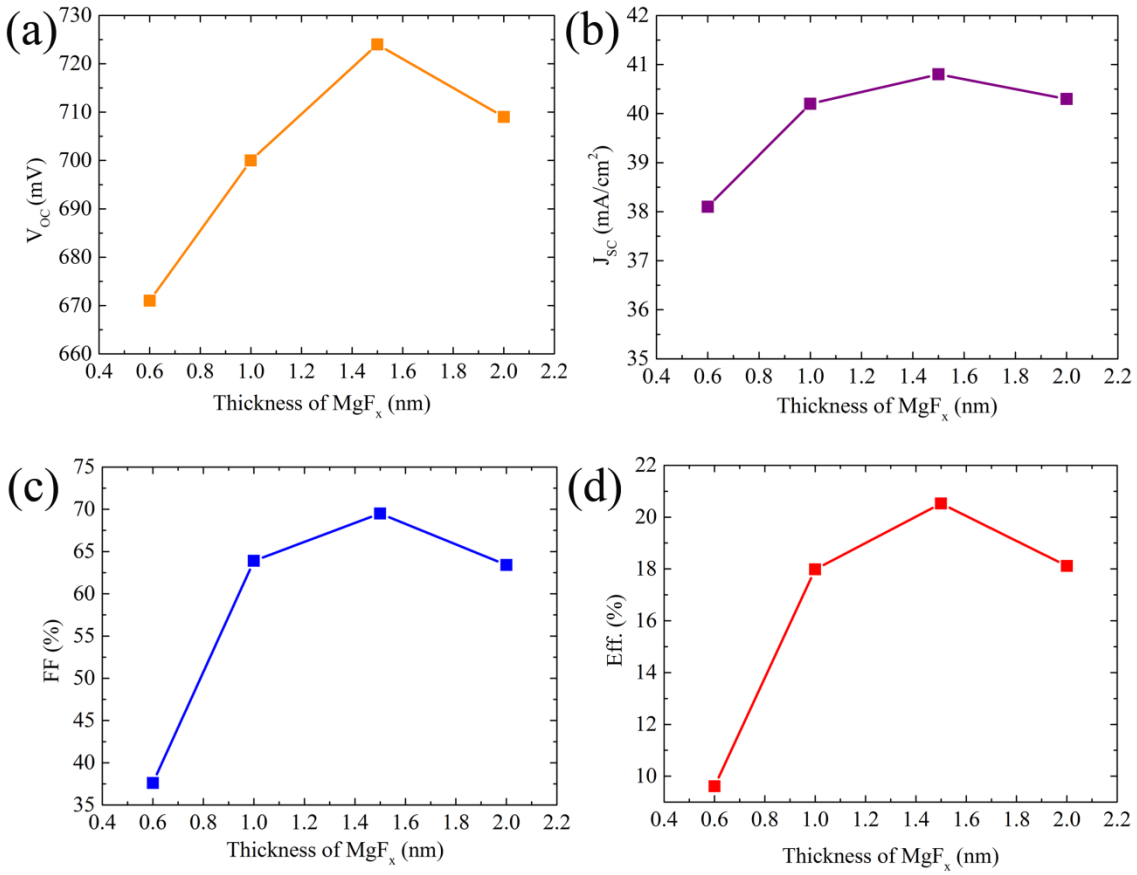

FIGURE 3. The characterized J-V parameters of small size IBC solar cells as functions of different thickness of MgF_x/Al as electron selective contact.

Table 1 shows the measured characteristic parameters of IBC devices using different electron-selective materials. The thickness of LiF_x, MgF_x, MgO_x are all kept as 1.5 nm, revealing that the work function is not the only parameter that will influence the carrier selectivity. Using MgF_x as electron-selective contact gives the largest V_{OC} of 724 mV. Interestingly, Ca metal directly evaporated on the rear-side a-Si:H (i) layer behaves as a severe Schottky diode, which leads to a S-shape J-V curve, resulting in a power conversion efficiency of only 1.8%. This behavior is similar with the rectifying contact of Al/a-Si:H/n-Si, and is mainly ascribed to the oxidation of Ca exposed in air. By contrast, the insertion of a Mg layer enhances substantially the cell performance, leading to a conversion efficiency of 14.5%.

After the optimization, MgF_x/SiN_x/a-Si:H is selected as front anti-reflection and passivation layers, MoO_x and MgF_x/Al as hole- and electron-selective contacts, respectively. Both were capped with Ag to make the fingers conductive enough. When illuminating the whole device area, a high V_{OC} of 709 mV is obtained, confirming that the intrinsic a-Si:H/MgF_2 shows excellent passivation. Good J_{SC} of 41.5 mA/cm^2 is also obtained, indicating little electrical shading, but *FF* is lower than 80% due to series resistance, leading to a highest efficiency of 22.2% shown in Table 2. The pseudo J-V curve was also measured and shown in Figure 4 (a) indicating a diode characteristic without shunt. Due to the thin Ag (800 nm) of IBC solar cell, series resistance is still large, causing relatively low FF as shown in Fig. 4 (a). The pseudo FF (pFF: FF excluding R_S power loss) of 84.2% and pseudo efficiency (efficiency excluding R_S power loss) of 24.8% are measured.Fig. 4 (b) shows the external quantum efficiency (EQE) and internal quantum efficiency (IQE) curves, along with measured reflectance. The cell exhibits very low front reflection and has outstanding collection efficiency, the IQE reach 98.2% - 99% ranging from 600 to 900-nm due to low recombination of MoO_x and MgF_x contacts. IQE stays also very high in the short wavelength range, suggesting that a significant part of the light absorbed in the front a-Si:H layer contributes to photogeneration contrarily to 2-side contacted devices [11].

TABLE 1. Characteristic parameters of dopant-free IBC solar cells prepared with different electron-selective contacts. The active area is 0.84 cm^2. The capping metal consists of a 70 nm Al / 500 nm Ag stack.

Electron contact	E_F (eV)	V_{OC} (mV)	J_{SC} (mA/cm^2)	*FF* (%)	*Eff.* (%)
LiF_x	2.8	710	39.1	43.5	12.1
MgF_x	3.5	724	40.1	69.5	20.2
MgO	4.1	663	40.3	48.2	12.9
Ca	2.9	495	21.3	17.1	1.8
Mg	3.7	642	40.1	55.5	14.5

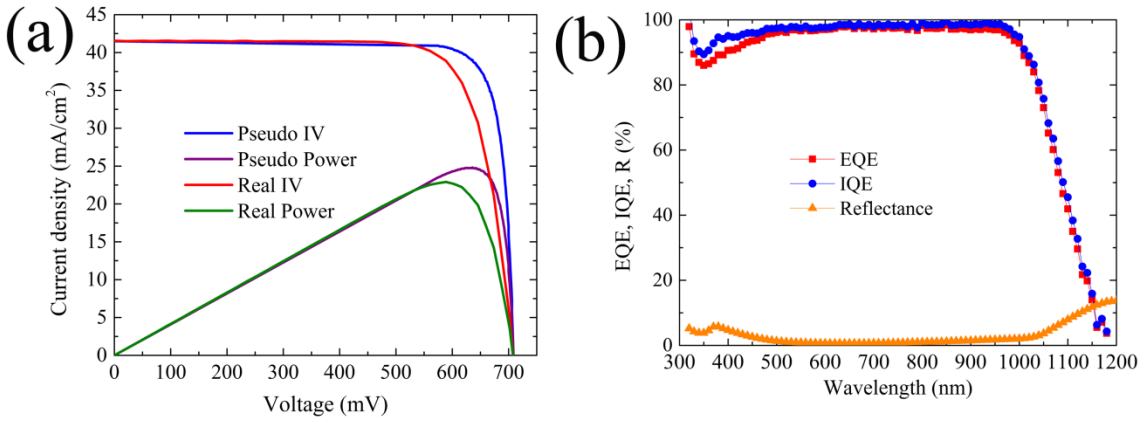

FIGURE 4. (a) The reflectance of IBC solar cells (A = 4.5 cm^2) with different antireflection films; (b) Implied open-circuit voltage (*i*-V_{oc}) values extracted from measured effective lifetime considering different front-side films.

The EQE loss in the short wavelength range is due to the front surface reflection loss and parasitic absorption of the a-Si:H (i) layer from the front side. The EQE loss in the long wavelength range is due to the strong parasitic absorption originating from the close vicinity of the metal electrodes to the wafer surfaces [12]. Further improvement would rely on introducing a rear side reflector.

TABLE 2. Characteristic parameters of dopant-free IBC solar cells were measured under standard test conditions (AM1.5G, 100 mW/cm^2, and 25 °C). The aperture cell area (A) is 4.5 cm^2.

A *[cm^2]*	V_{oc} *[mV]*	J_{sc} *[mA/cm2]*	*FF* *[%]*	η *[%]*	*pFF* *[%]*
4.5	709	41.5	75.6	22.2	84.2

CONCLUSION

Efficient a-Si:H-passivated, dopant-free, back-contacted solar cells were fabricated with a simple 2-mask 1-alignment process. V_{oc} as high as 709 mV was measured, together with J_{sc} of 41.5 mA/cm^2 and FF up to 75.6%. Efficiency is limited to 22.2% by large series resistance partly due to the thin evaporated metal used as electrode but presumably mostly due to large contact resistances (pseudo-efficiency up to 25% are obtained). The effect of varying the MgF_x film thickness as the electron contact layer on the rear side was also investigated, and an optimal thickness

of 1.5 nm was identified for high V_{OC} and *FF*. We compared different electron-selective contact materials including Mg-based and fluoride materials and discuss the suitable combinations. Further work include unravelling the influence of the thickness and nature of the electron-selective layer and of the type and thickness of the capping metal layer. Thicker evaporated metal or alternative metallization will also be investigated to exploit fully the potential of this approach.

ACKNOWLEDGMENTS

This work was supported by the National Natural Science Foundation (Contract No. 61774173), the International Program for Ph.D. Candidates Sun Yat-Sen University (Grant No. 02300-18827001), and the Jiangsu Collaborative Innovation Center of Photovoltaic Science and Engineering (Grant No. SCZ1405500002). This project has received funding from the European Union's Horizon 2020 research and innovation programme under Grant Agreement No. 727523 (NextBase).

REFERENCES

1. Lammert, Michael D., and Richard J. Schwartz, IEEE Transactions on Electron Devices **24**, 337-342 (1977).
2. Smith. D. D, Reich. G., Baldrias. M, Reich. M, Boitnott. N and Bunea. G, In Photovoltaic Specialists Conference (PVSC), IEEE **43**, 3351-3355 (2016).
3. Battaglia Corsin, Andres Cuevas, and Stefaan De Wolf, Energy & Environmental Science **9**, 1552-1576 (2016).
4. Franklin. E, Fong. K, McIntosh. K, Fell. A, Blakers. A, Kho. T and Wang. E. C, Progress in Photovoltaics: research and applications, 24(4), 411-427.
5. Dahlinger, M, Carstens, K, Hoffmann, E, Zapf Gottwick, R., & Werner, J. H., 23.2% laser processed back contact solar cell: fabrication, characterization and modeling. Progress in Photovoltaics: Research and Applications **25**, 192-200 (2017).
6. Zieliński. B, O'Sullivan. B. J, Singh. S, de Castro, A. U, Li. Y, Jambaldinni. S and Poortmans. J, Solar Energy Materials and Solar Cells **163**, 66-72 (2017).
7. Chen. Y, Yang. Y, Marmon. J. K, Zhang. X, Feng. Z, Verlinden. P. J and Shen, H, IEEE Journal of Photovoltaics **7**, 51-5 (2017)
8. Wu W, Lin W, Bao J, Liu Z, Liu B, Qiu K and Shen, H, RSC Advances **7**, 23851-23858 (2017).
9. Bullock. J, Hettick. M, Geissbühler. J, Ong. A. J, Allen. T, Sutter-Fella. C. M and Ballif, C, Nature Energy **1**, 15031 (2016).
10. https://www.pvlighthouse.com.au.
11. Holman, Z.C., Descoeudres, A., Barraud, L., Fernandez, F.Z., Seif, J.P., De Wolf, S. and Ballif, C., IEEE Journal of Photovoltaics **2**, 7-15 (2012).
12. Holman, Z.C., De Wolf, S. and Ballif, C., Light: Science & Applications **2**, 106. (2013).
13. Jorge, P., Marie, J., Angélique, B., Eric, T., Daniel, L., Progress in Photovoltaics: Research and Applications, 1-9 (2018).
14. Yimao, W., Chris, S., James, B., Thomas, A., Mark, H., Di, Y., Peiting, Z., Xinyu, Z., Jie, C., Josephine, M., Ali, J. and Andres, C., ACS Applied Materials & Interfaces 10, 13645–13651, (2018).